

Optical STAR-RIS-Aided VLC Systems: RSMA Versus NOMA

Omar Maraqa, Sylvester Aboagye, *Member, IEEE*, and Telex M. N. Ngatched, *Senior Member, IEEE*

Abstract—A critical concern within the realm of visible light communications (VLC) pertains to enhancing system data rate, particularly in scenarios where the direct line-of-sight (LoS) connection is obstructed by obstacles. The deployment of meta-surface-based simultaneous transmission and reflection reconfigurable intelligent surface (STAR-RIS) has emerged to combat challenging LoS blockage scenarios and to provide 360° coverage in radio-frequency wireless systems. Recently, the concept of optical simultaneous transmission and reflection reconfigurable intelligent surface (OSTAR-RIS) has been promoted for VLC systems. This work is dedicated to studying the performance of OSTAR-RIS in detail and unveiling the VLC system performance gain under such technology. Specifically, we propose a novel multi-user indoor VLC system that is assisted by OSTAR-RIS. To improve the sum rate performance of the proposed system, both power-domain non-orthogonal multiple access (NOMA) and rate splitting multiple access (RSMA) are investigated in this work. To realize this, a sum rate maximization problem that jointly optimizes the roll and yaw angles of the reflector elements as well as the refractive index of the refractor elements in OSTAR-RIS is formulated, solved, and evaluated. The maximization problem takes into account practical considerations, such as the presence of non-users (i.e., blockers) and the orientation of the recipient's device. The sine-cosine meta-heuristic algorithm is employed to get the optimal solution of the formulated non-convex optimization problem. Moreover, the study delves into the sum energy efficiency optimization of the proposed system. Simulation results indicate that the proposed OSTAR-RIS RSMA-aided VLC system outperforms the OSTAR-RIS NOMA-based VLC system in terms of both the sum rate and the sum energy efficiency.

Index Terms—Visible light communication (VLC), optical simultaneous transmission and reflection reconfigurable intelligent surface (OSTAR-RIS), reflecting intelligent surface (RIS), rate splitting multiple access (RSMA), non-orthogonal multiple access (NOMA).

I. INTRODUCTION

THE rapid growth in the number of interconnected devices and the continuous advancement of wireless applications are prompting the exploration of alternative wireless communication solutions beyond radio frequency (RF) communications. Visible light communications (VLC) is a technology that uses visible light to communicate, and has many advantages such as being cost-efficient, bandwidth-abundant, and highly-secured [1]. Consequently, VLC is regarded as a promising

complementary technology to RF communications within upcoming wireless networks [1].

Reliable data transmission in VLC systems requires a clear line-of-sight (LoS) path between the transmitter and the receiver [2]. Nevertheless, this direct path can be blocked due to factors such as the presence of other users (i.e., blockers), obstacles within indoor environments, or the orientation of the recipient's device. Many previous investigations into VLC systems neglected to account for the impact of random device orientations, even though this is a crucial consideration for practical VLC system design and evaluation.

In another development, in the last couple of years, researchers have proposed the deployment of reflecting intelligent surfaces (RISs) on walls to enhance the quality of the communication links in VLC systems and to combat the LoS blockage. In instances where the LoS path is obstructed, an RIS can steer the light propagation in the wireless channel to overcome the blockage. Therefore, the integration of RIS technology can reduce the reliance of VLC systems on LoS paths. Two main streams have evolved concerning the adoption of RIS in VLC systems, namely, mirror array-based RIS [2]–[16] and meta-surface-based RIS [17]–[22]. The authors in [24] observed that the mirror array-based RIS demonstrates superior performance gains compared to the meta-surface-based RIS.

To provide 360° coverage and to combat challenging LoS blockage scenarios, meta-surface-based simultaneous transmission and reflection reconfigurable intelligent surface (STAR-RIS) was investigated for VLC systems in [23]. As a result of the more recent developments in the STAR-RIS materials, the concept and the fabrication method of optical simultaneous transmission and reflection reconfigurable intelligent surface (OSTAR-RIS) are presented in [25]. The proposed OSTAR-RIS consists of liquid crystal (LC)-based RIS that can be designed to act as reflectors or/and refractors.

On the other hand, in a separate development, a new interference management approach referred to as rate splitting multiple access (RSMA) [26], [27] has been gaining attention for its ability to enhance the spectral efficiency within a wide range of interference scenarios. RSMA has been demonstrated to embrace and outperform existing multiple access schemes, namely, orthogonal multiple access (OMA), space division multiple access based on linear precoding, physical layer multicasting, and non-orthogonal multiple access (NOMA) based on linear superposition coding with successive interference cancellation (SIC) [27].

In this work, a novel multi-user indoor VLC system that is assisted by OSTAR-RIS is presented, optimized, and eval-

Omar Maraqa and Telex M. N. Ngatched are with the Department of Electrical and Computer Engineering, McMaster University, Hamilton, Canada (e-mail: dr.omar.maraqa@gmail.com; ngatchet@mcmaster.ca). Sylvester Aboagye is with the Department of Electrical Engineering and Computer Science, York University, Toronto, Canada (e-mail: aboagye@yorku.ca).

This work has been submitted to the IEEE for possible publication. Copyright may be transferred without notice, after which this version may no longer be accessible.

Table I

STATE-OF-THE-ART RIS-AIDED OPTIMIZED SOLUTIONS IN VLC SYSTEMS. (“ASNRR”:“AVERAGE SIGNAL-TO-NOISE RATIO”, “BER”:“BIT ERROR RATE”, “MSE”:“MEAN SQUARE ERROR”)

[#]	RIS type				Objective function							Access technique		
	Meta-surface-based RIS	Mirror array-based RIS	STAR-RIS (Meta-surface-based RIS)	OSTAR-RIS (Liquid crystal and mirror array-based RIS)	ASNRR	MSE	BER	Secrecy Rate	Secrecy EE	Rate	EE	OMA	NOMA	RSMA
[2]		✓								✓		✓		
[3]		✓								✓		✓		
[4]		✓						✓				✓		
[5]		✓						✓					✓	
[6]		✓								✓		✓		
[7]		✓				✓						✓		
[8]		✓								✓		✓		
[9]		✓					✓					✓		
[10]		✓			✓							✓		
[11]		✓						✓				✓		
[12]		✓						✓				✓		
[13]		✓									✓	✓		
[14]		✓								✓		✓		
[15]		✓							✓			✓		
[16]		✓								✓	✓	✓	✓	
[17]	✓									✓		✓		
[18]	✓									✓	✓	✓		
[19]	✓									✓		✓	✓	
[20]	✓						✓						✓	✓
[21]	✓									✓			✓	
[22]	✓								✓			✓		
[23]			✓							✓	✓		✓	
Proposed solution				✓						✓	✓		✓	✓

uated. Unlike the design in [25], our OSTAR-RIS is made of both LC-based RIS and mirror-array based RIS. For the reader’s convenience, Table I summarizes the most related works and compares them to our proposed work according to (i) the adopted RIS type, (ii) optimized objective function, and (iii) adopted multiple access technique. From this table, it is visible that most of the works have considered OMA-based schemes, some works have considered power-domain NOMA scheme to boost the achievable rate in VLC systems, but none has considered the RSMA scheme. To the best of the authors’ knowledge, this is the first work that technically evaluates OSTAR-RIS under the RSMA scheme.

Our contributions can be listed as follows:

- A novel multi-user indoor VLC system that is assisted by OSTAR-RIS is proposed. The proposed system accounts for both the effect of the orientation of the user’s device and the non-user blockers.
- A sum rate optimization problem for both the power-domain NOMA scheme and the RSMA scheme is formulated while jointly designing the yaw and roll angles of the mirror array-based OSTAR-RIS elements as well as the refractive index of the LC-based OSTAR-RIS elements. The sine-cosine meta-heuristic algorithm is utilized to get the global optimal solution for the formulated multi-variate non-convex optimization problem.
- A sum energy efficiency (SEE) optimization problem for both the power-domain NOMA scheme and the RSMA scheme is also formulated and solved, given the significance of this metric in assessing VLC systems.
- Detailed simulation results are provided to demonstrate the superiority of the RSMA scheme over the power-domain NOMA scheme for the proposed system in terms

of both the sum rate and the SEE metrics while considering different network parameters, such as the access point (AP) optical transmit power, the wavelength of the transmitted light, the number of elements in the OSTAR-RIS, and the number of served users. In addition, the effect of adopting different power allocation strategies on the sum rate performance of the RSMA scheme is illustrated.

The organization of the rest of this paper is as follows. In Section II, the system and channel models of the proposed OSTAR-RIS-aided VLC system that considers both LC-based OSTAR-RIS elements and mirror array-based OSTAR-RIS elements are presented. The analysis of both adopted multiple access schemes (i.e., power-domain NOMA scheme and RSMA scheme) are provided in Section III. In Section IV, the sum rate maximization problem for both aforementioned multiple access schemes is formulated and optimally solved using the sine-cosine meta-heuristic algorithm. In Section V, a SEE optimization of the proposed system is given. Detailed Simulation results are provided in Section VI. Finally, the paper conclusion is given in Section VII.

II. SYSTEM AND CHANNEL MODELS

In this section, the system and channel models of the proposed OSTAR-RIS-aided VLC system are presented.

A. Indoor VLC System

An indoor downlink VLC system with a single light emitting diode (LED) array as the AP and multiple users is illustrated in Fig. 1. In this figure, the indoor environment is partitioned into two compartments, with multiple users

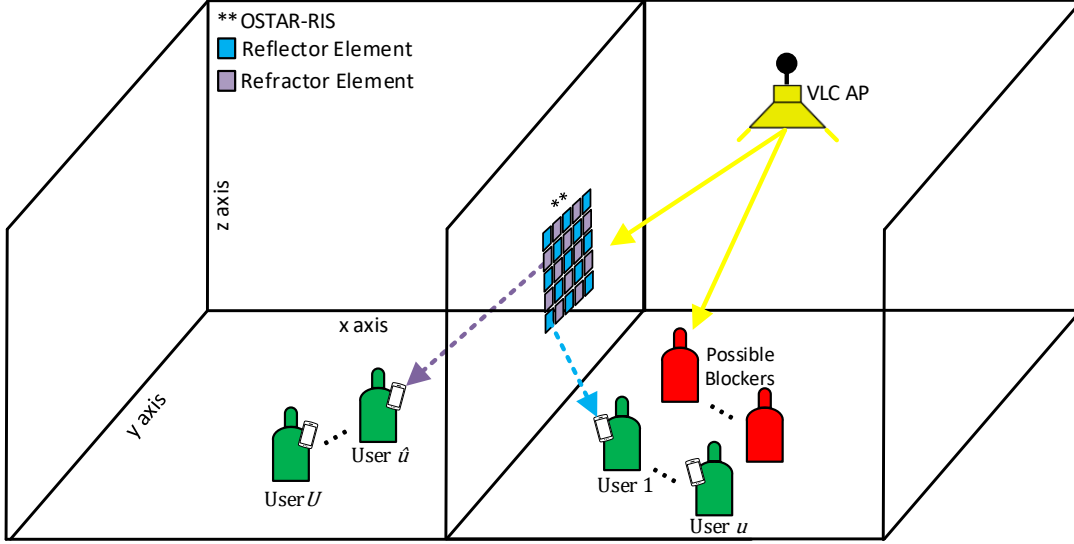


Fig. 1. Illustrations of the proposed OSTAR-RIS-aided VLC system.

deployed on each side. Due to room design requirements (e.g., functional design where one compartment is intended as a workspace and the other for relaxation or sleeping, architectural constraints, and individual preferences), one compartment has an LED array installed while the other does not have any light fixture. Multiple non-users present in the indoor environment may block the LoS signal from the VLC AP (i.e., non-user blockers). Moreover, we consider self-blockage, which occurs when (i) a user's body blocks the light path to the receiving device or (ii) with random device orientation. To enable wireless data transmission in the compartment without the LED array, support non-LoS transmissions, and overcome the impact of device orientation on the achievable data rate, an OSTAR-RIS is deployed on the wall separating the two compartments.

The OSTAR-RIS is composed of mirror array-based RISs and LC-based RISs, that have been interleaved as shown in Fig. 1. The mirror array RISs act as reflector elements that reflect and steer incident light to the users. The LC-based RISs serve as refractor elements that amplify, refract/transmit, and steer any incident signal to users in the other compartment. The purple dotted and blue dotted lines in the figure denote the refracted light signal and the reflected signal, respectively.

B. VLC Channel

The channel gain between the AP and the users can be expressed as

$$H = \begin{cases} \iota H_{\text{LoS}} + \sum_{k=1}^{\mathcal{K}} H_{\text{NLoS}}^{\text{RIS}_k}, & \text{if the user lies in Room 1} \\ \sum_{n=1}^{\mathcal{N}} H_{\text{NLoS}}^{\text{RIS}_n} \times \psi_{\text{LC}}, & \text{if the user lies in Room 2} \end{cases} \quad (1)$$

where "Room 1" and "Room 2" denote the compartments with and without the VLC AP, respectively, $\iota \in \{0, 1\}$ is an indicator function for the presence or absence of a LoS path, H_{LoS} represent the channel gain of the LoS path, $H_{\text{NLoS}}^{\text{RIS}_k}$ is the non-line-of-sight (NLoS) channel gain of the reflected signal from the k -th reflector element, $H_{\text{NLoS}}^{\text{RIS}_n}$ represents the NLoS channel gain of the refracted signal from the n -th refractor element, and ψ_{LC} is the transition coefficient for the

refractor element that characterizes the propagation of light signal through the LC-based RIS elements.

The channel gain for the LoS path can be given as [28]

$$H_{\text{LoS}} = \begin{cases} \frac{(m+1)A_{\text{PD}}}{2\pi d^2} G(\xi) T(\xi) \cos^m(\Phi) \cos(\xi), & 0 \leq \xi \leq \xi_{\text{FoV}} \\ 0, & \xi > \xi_{\text{FoV}} \end{cases} \quad (2)$$

where $m = -(\log_2(\cos(\Phi_{1/2})))^{-1}$ is the Lambertian order of emission with $\Phi_{1/2}$ as the semi-angle at half power of the LED, A_{PD} is the detector physical area of the photo-diode (PD), d is the link distance, Φ denotes the radiation angle, ξ is the incident angle, $T(\xi)$ is the gain of the optical filter, and $G(\xi) = f^2 / \sin^2 \xi_{\text{FoV}}$ is the optical gain of the non-imaging concentrator with an internal refractive index f . In (2), the cosine of ξ captures the impact of random device orientation on the signal propagation and can be expressed as [29]

$$\cos(\xi) = \left(\frac{x_a - x_u}{d}\right) \cos(\beta) \sin(\alpha) + \left(\frac{y_a - y_u}{d}\right) \sin(\beta) \sin(\alpha) + \left(\frac{z_a - z_u}{d}\right) \cos(\alpha), \quad (3)$$

where (x_a, y_a, z_a) and (x_u, y_u, z_u) are the position vectors for the locations of the AP and the user, respectively, and α and β denote the polar and azimuth angles of the receiver, respectively.

1) Mirror Array-Based OSTAR-RIS-Aided VLC Channel:

The channel gain of the NLoS path considering signal propagation from the AP to the k -th mirror having an area dA_k and reflection from the k -th mirror to the u -th user in Room 1 can be given as [24]

$$H_{\text{NLoS}}^{\text{RIS}_k} = \begin{cases} \rho_{\text{RIS}} \frac{(m+1)A_{\text{PD}}}{2\pi^2 (d_k^a)^2 (d_k^u)^2} dA_k G(\xi) T(\xi) \cos^m(\Phi_k^a) \\ \times \cos(\xi_k^a) \cos(\Phi_k^u) \cos(\xi_k^u), & 0 \leq \xi_k^u \leq \xi_{\text{FoV}} \\ 0, & \xi_k^u > \xi_{\text{FoV}} \end{cases} \quad (4)$$

where ρ_{RIS} denotes the reflectivity of the RIS, d_k^a and d_k^u are the link distance for AP-RIS and RIS-user paths, respectively,

Φ_k^a is the radiation angle for the path from the AP to the k -th reflective surface, ξ_k^a is the incident angle for the path from the AP to k -th reflective surface, Φ_u^k is the angle of irradiance for the path from reflective surface k towards user u , and ξ_u^k is the incident angle of the reflected signal from surface k to user u . Note that $\cos(\xi_k^a)$ can be easily calculated using (3) to capture the effects of the random device orientation while $\cos(\Phi_u^k)$ can be expressed as [30]

$$\begin{aligned} \cos(\Phi_u^k) = & \left(\frac{x_k - x_u}{d_k^u} \right) \sin(\gamma) \cos(\omega) + \\ & \left(\frac{y_k - y_u}{d_k^u} \right) \cos(\gamma) \cos(\omega) + \\ & \left(\frac{z_k - z_u}{d_k^u} \right) \sin(\omega), \end{aligned} \quad (5)$$

with (x_k, y_k, z_k) being the position vector of the k -th reflecting element, and γ and ω are the yaw and roll angles of the mirror array-based RIS.

2) *Liquid Crystal-Based OSTAR-RIS-Aided VLC Channel:* The channel gain of the NLoS signal path for the signal propagation from the AP, through the n -th refracting element, and to the \hat{u} -th user in Room 2 is given as $H_{\text{NLoS}}^{\text{RIS}_n} \times \psi_{\text{LC}}$, where

$$H_{\text{NLoS}}^{\text{RIS}_n} = \begin{cases} \frac{(m+1)A_{\text{PD}}}{2\pi^2(d_n^a)^2(d_u^a)^2} dA_n G(\xi) T(\xi) \cos^m(\Phi_u^a) \\ \times \cos(\xi_n^a) \cos(\Phi_u^n) \cos(\xi_u^n), & 0 \leq \xi_u^n \leq \xi_{\text{FoV}} \\ 0, & \xi_u^n > \xi_{\text{FoV}} \end{cases}$$

$$\begin{aligned} \text{with } \cos(\Phi_u^n) = & \left(\frac{x_n - x_{\hat{u}}}{d_n^{\hat{u}}} \right) \sin(\gamma) \cos(\omega) + \\ & \left(\frac{y_n - y_{\hat{u}}}{d_n^{\hat{u}}} \right) \cos(\gamma) \cos(\omega) + \left(\frac{z_n - z_{\hat{u}}}{d_n^{\hat{u}}} \right) \sin(\omega), \end{aligned} \quad (6)$$

where (x_n, y_n, z_n) is the location of the n -th refracting element. On the other hand, the transition coefficient of any refracting element, ψ_{LC} , can be given by [30]

$$\psi_{\text{LC}} = T_{\text{ac}}(\xi_u^n) \times T_{\text{ca}}(\theta), \quad (7)$$

where $T_{\text{ac}}(\xi_u^n)$ and $T_{\text{ca}}(\theta)$ represent the angular transmittance as the optical signal enters and exits the LC cell. Since none of the incident light signals get absorbed at the surface of the LC cell, the angular transmittance can be expressed in terms of the angular reflectance as $T_{\text{ac}}(\xi_u^n) = (1 - R_{\text{ac}}(\xi_u^n))$ and $T_{\text{ca}}(\theta) = (1 - R_{\text{ca}}(\theta))$. According to [30], the angular reflectance can be derived as

$$\begin{aligned} R_{\text{ac}}(\xi_u^n) = & \frac{1}{2} \left(\frac{\eta^2 \cos(\xi_u^n) - \sqrt{\eta^2 - \sin^2(\xi_u^n)}}{\eta^2 \cos(\xi_u^n) + \sqrt{\eta^2 - \sin^2(\xi_u^n)}} \right)^2 + \\ & \frac{1}{2} \left(\frac{\cos(\xi_u^n) - \sqrt{\eta^2 - \sin^2(\xi_u^n)}}{\cos(\xi_u^n) + \sqrt{\eta^2 - \sin^2(\xi_u^n)}} \right)^2, \end{aligned} \quad (8)$$

$$\begin{aligned} R_{\text{ca}}(\theta) = & \frac{1}{2} \left(\frac{\cos(\theta) - \sqrt{\eta_1^2 - \sin^2(\theta)}}{\cos(\theta) + \sqrt{\eta_1^2 - \sin^2(\theta)}} \right)^2 + \\ & \frac{1}{2} \left(\frac{\eta_1^2 \cos(\theta) - \sqrt{\eta_1^2 - \sin^2(\theta)}}{\eta_1^2 \cos(\theta) + \sqrt{\eta_1^2 - \sin^2(\theta)}} \right)^2, \end{aligned} \quad (9)$$

where $\eta = \eta_c/\eta_a$ and $\eta_1 = \eta_a/\eta_c$ are the relative refractive indices with η_c and η_a being the refractive indices of the LC cell and air, respectively. It can be observed from (7) to (9) that the transition coefficient ψ_{LC} can be optimized by tuning the refractive index of the LC cell η_c . According to [31], tuning the refractive index involves adjusting the tilt angle of the LC molecules (i.e., molecular orientation) by applying an external electric field. Mathematically, the relation between the tilt angle Ξ of an LC molecule and the refractive index of the LC cell is given by

$$\frac{1}{\eta_c^2(\Xi)} = \frac{\cos^2(\Xi)}{\eta_e^2} + \frac{\sin^2(\Xi)}{\eta_o^2}, \quad (10)$$

where η_o and η_e denote the LC cell's ordinary and extraordinary refractive indices, respectively. The tilt angle can also be expressed as a function of the externally applied voltage V_E as [30]

$$\Xi = \begin{cases} 0, & V_E \leq V_{\text{TH}} \\ \frac{\pi}{2} - 2 \tan^{-1} \left[\exp \left(\frac{V_{\text{TH}} - V_E}{V_0} \right) \right], & V_E > V_{\text{TH}} \end{cases} \quad (11)$$

where V_{TH} is the critical voltage threshold above which the tilting process begins.

In addition to its light steering capability, LC-based RIS can be used to provide light amplification for the emerging signal through the process of stimulated emission. In this process, the incident photons interact with the excited molecules (via an external voltage) of the LC cell. This causes the molecules to drop to a lower energy level, creating new identical photons. When an optical signal of power P_{in} impinges on an LC cell with the transition coefficient ψ_{LC} , the output signal power after undergoing light amplification in the presence of an external electric field can be calculated using the Beer's absorption law as [32]

$$P_{\text{out}} = P_{\text{in}} \times \exp(\Gamma D) \times \psi_{\text{LC}}, \quad (12)$$

where Γ is the amplification gain coefficient, which is given as [33]

$$\Gamma = \frac{2\pi\eta_c^3}{\cos(\xi_u^n)\lambda} r_{\text{eff}} E, \quad (13)$$

D denotes the depth of the LC cell, and the term $\exp(\Gamma D)$ represents the exponential increase of the incident signal power. In (13), λ represents the optical signal's wavelength, E [V/m] is the external electric field, and r_{eff} is the electro-optic coefficient. It can be observed from (13) that the amplification capability of the LC-based RIS depends on the refractive index η_c , the wavelength λ , and the external electric field. However, the external electric field $E = V_E/D$ and the refractive index of the LC-cell are related through (10) and (11). Specifically,

$$V_E = V_{\text{TH}} - \log \left(- \tan \left[\frac{\tan^{-1} \left(\frac{\eta_o \sqrt{(\eta_e^2 - \eta_o^2)(\eta_e^2 - \eta_c^2)}}{\eta_c(\eta_e^2 - \eta_o^2)} \right)}{2} - \frac{\pi}{4} \right] \right). \quad (14)$$

As a result, we focus on optimizing the refractive index to maximize the amplification gain coefficient for a given optical signal of wavelength λ .

III. ADOPTED MULTIPLE ACCESS SCHEMES

This work investigates two multiple access schemes, namely, power-domain NOMA and RSMA to boost the sum rate of the proposed system. While implementing these schemes, the number of intended users is assumed to be U and they have been sorted in order of their channel gain $H_1 \geq \dots \geq H_u$ and $H_{\hat{u}} \geq \dots \geq H_U$ [34].

A. Power-domain NOMA Scheme

Following the power-domain NOMA scheme [35], using the superposition coding principle, the AP sends a superposed signal to the intended users, which is given as [16]

$$x^{\text{NOMA}} = \left(\sum_{u=1}^U \sqrt{c_u P_S} s_u \right) + I_{\text{DC}}, \quad (15)$$

where P_S denotes the electrical transmission power of the signal (P_S is equal to $(\frac{p}{q})^2$ [16], here p represents the optical power and q symbolizes the electrical to optical conversion ratio), s_u denotes the modulated message signal meant for the u -th user, I_{DC} is a constant bias current introduced to guarantee a positive instantaneous intensity [36], and c_u denotes the NOMA power allocation ratio and is given by [16]

$$c_u = \begin{cases} \mu^{\text{NOMA}} (1 - \mu^{\text{NOMA}})^{u-1}, & \text{if } 1 \leq u < U \\ (1 - \mu^{\text{NOMA}})^{u-1}, & \text{if } u = U \end{cases} \quad (16)$$

where μ^{NOMA} is a constant that falls within the range of $(0.5, 1]$ and $\sum_{u=1}^U c_u = 1$ [37]. After removing the DC bias, the signal received by the u -th user can be represented as [16]

$$y_u^{\text{NOMA}} = H_u \times \left(\sum_{u=1}^U \sqrt{c_u P_S} s_u \right) + z_u, \quad (17)$$

where $z_u \sim \mathcal{N}(0, \sigma^2)$ is the additive real-valued Gaussian noise with variance σ^2 . Both the shot and thermal noises are included in z_u . According to the power-domain NOMA scheme [35], through SIC, each user can decode its information. Subsequently, the sum rate of the proposed system under the power-domain NOMA scheme is given by

$$R_{\text{sum}}^{\text{NOMA}} = \sum_{u=1}^U R_u,$$

with

$$R_u = \begin{cases} B \log_2 \left(1 + \frac{\exp(1)}{2\pi} \frac{(R_{\text{PD}} H_i)^2 c_i P_S}{I_{\text{Room } 1} + N_o B} \right), & 1 \leq i < u \\ B \log_2 \left(1 + \frac{\exp(1)}{2\pi} \frac{(R_{\text{PD}} \exp(\Gamma D) H_i)^2 c_i P_S}{I_{\text{Room } 2} + N_o B} \right), & \hat{u} \leq i < U \\ B \log_2 \left(1 + \frac{\exp(1)}{2\pi} \frac{(R_{\text{PD}} \exp(\Gamma D) H_i)^2 c_i P_S}{N_o B} \right), & i = U \end{cases} \quad (18)$$

where N_o represents the noise power spectral density, B represents the system's bandwidth, both $I_{\text{Room } 1} = (R_{\text{PD}} H_i)^2 \sum_{j=i+1}^U c_j P_S$ and $I_{\text{Room } 2} = (R_{\text{PD}} \exp(\Gamma D) H_i)^2 \sum_{j=i+1}^U c_j P_S$ represent the inter-user interference terms in Room 1 and Room 2, respectively.

B. RSMA Scheme

For implementing this scheme, the 1-layer RSMA [38]–[40] is employed. In this scheme, a user's message is split into both a private part and a common part. The VLC AP combines all users' common parts into a single message, which is encoded into a common stream. This common stream is broadcast to all users alongside each user's private stream. Every user can decode the common stream, whereas each user only needs to decode their respective private stream. At the user-side, through the deployment of SIC, the common stream is eliminated, allowing the user to decode their private stream, treating the private streams of other users as noise [39]. Accordingly, the VLC AP transmitted power is divided as

$$P_S = P_0 + \sum_{u=1}^U P_u, \quad (19)$$

where P_0 is the transmit power of the common stream and P_u is the transmit power of the private stream intended for the u -th user. In this scheme, for a user to successfully decode its private stream, after subtracting the common stream, the difference between the common stream's power and the private streams' power should satisfy the following constraint [39]

$$P_0 \delta_u - \sum_{u=1}^U P_u \delta_u \geq P_{\text{tol}}, \quad (20)$$

where $\delta_u = \frac{|H_u|^2}{N_o}$ and P_{tol} is the SIC threshold that guarantee the successful decoding of messages in RSMA scheme. Based on (20), the AP allocates a portion of its total power to the common stream (i.e., $P_0 = \mu^{\text{RSMA}} P_S$) and the other portion to the private streams (i.e., $\sum_{u=1}^U P_u = (1 - \mu^{\text{RSMA}}) P_S$), where $\mu^{\text{RSMA}} \in (0, 1)$ [41]. The aforementioned portion of power dedicated to private streams is divided equally between users. In the simulation section, we show that the adopted power allocation (i.e., equal power allocation) strategy is better performance-wise than both (i) the NOMA-alike power allocation strategy (i.e., distributing the power using the same strategy utilized in the NOMA scheme based on (16)) and (ii) the random power allocation. The VLC AP transmitted signal is given as [38]

$$x^{\text{RSMA}} = \sqrt{P_0} s_c + \sum_{u=1}^U \sqrt{P_u} s_u + I_{\text{DC}}, \quad (21)$$

where s_c denotes the common stream, s_u denotes the private stream intended for the u -th user, and I_{DC} is a constant bias current. At the u -th user, the total received signal is

$$y_u^{\text{RSMA}} = H_u \times \left(\sqrt{P_0} s_c + \sum_{u=1}^U \sqrt{P_u} s_u \right) + z_u. \quad (22)$$

Accordingly, the rate of the u -th user decoding the common stream is given as

$$R_{c,u} = \begin{cases} B \log_2 \left(1 + \frac{\exp(1)}{2\pi} \frac{(R_{\text{PD}} H_i)^2 P_0}{I_{\text{Room } 1}^{\text{Common}} + N_o B} \right), & 1 \leq i < u \\ B \log_2 \left(1 + \frac{\exp(1)}{2\pi} \frac{(R_{\text{PD}} \exp(\Gamma D) H_i)^2 P_0}{I_{\text{Room } 2}^{\text{Common}} + N_o B} \right), & \hat{u} \leq i \leq U \end{cases} \quad (23)$$

where both $I_{\text{Room 1}}^{\text{Common}} = (R_{\text{PD}}H_i)^2 \sum_{j=1}^U P_j$ and $I_{\text{Room 2}}^{\text{Common}} = (R_{\text{PD}}\exp(\Gamma D)H_i)^2 \sum_{j=1}^U P_j$ represent an inter-user interference terms, resulting from the application of the RSMA scheme, in Room 1 and Room 2, respectively.

To ensure the successful decoding of the common stream by all users, based on the assumed channel ordering, we should choose the rate of the common stream to be $R_{c,U}$ [38], which can be represented as

$$\begin{aligned} \min_{1 \leq u \leq U} R_{c,u} &= R_{c,U} \\ &= B \log_2 \left(1 + \frac{\exp(1)}{2\pi} \times \frac{(R_{\text{PD}}\exp(\Gamma D)H_U)^2 P_0}{(R_{\text{PD}}\exp(\Gamma D)H_U)^2 \sum_{j=1}^U P_j + N_o B} \right). \end{aligned} \quad (24)$$

Given that the rate of the common stream is $R_{c,U}$, the total data rates of all users receiving the common stream must be less than or equal $R_{c,U}$. This relation can be expressed as [38]

$$\sum_{u=1}^U R_{c,u} \leq R_{c,U}, \quad (25)$$

where, based on Lemma 1 in [38], the optimal solution for the rate of the common stream is obtained at the equality of (25).

At each user, the rate of decoding the private stream is

$$R_{p,u} = \begin{cases} B \log_2 \left(1 + \frac{\exp(1)}{2\pi} \frac{(R_{\text{PD}}H_i)^2 P_i}{I_{\text{Room 1}}^{\text{Private}} + N_o B} \right), & 1 \leq i < u \\ B \log_2 \left(1 + \frac{\exp(1)}{2\pi} \frac{(R_{\text{PD}}\exp(\Gamma D)H_i)^2 P_i}{I_{\text{Room 2}}^{\text{Private}} + N_o B} \right), & \hat{u} \leq i \leq U \end{cases} \quad (26)$$

where both $I_{\text{Room 1}}^{\text{Private}} = (R_{\text{PD}}H_i)^2 \sum_{j=1, j \neq u}^U P_j$ and $I_{\text{Room 2}}^{\text{Private}} = (R_{\text{PD}}\exp(\Gamma D)H_i)^2 \sum_{j=1, j \neq u}^U P_j$ represent also an inter-user interference terms in Room 1 and Room 2, respectively.

Subsequently, the sum rate of the proposed RSMA scheme is given by

$$R_{\text{sum}}^{\text{RSMA}} = \sum_{u=1}^U (R_{c,u} + R_{p,u}). \quad (27)$$

IV. SUM RATE OPTIMIZATION

In this section, the details of the sum rate optimization problem for both power-domain NOMA and RSMA schemes is presented. Also, the sine-cosine meta-heuristic algorithm is utilized to get the global optimal solution for the formulated multi-variate non-convex optimization problem.

A. Sum Rate Maximization Problem

The main purpose of this paper is to maximize the sum rate of the OSTAR-RIS-aided VLC system. To do so, the sum rate maximization problem that jointly optimizes the roll angle, ω ,

the yaw angle, γ , and the refractive index, η_c , of the OSTAR-RIS is considered and formulated as

$$(P0): \max_{\{\omega, \gamma, \eta_c\}} R_{\text{sum}}^{\text{NOMA}} \text{ or } R_{\text{sum}}^{\text{RSMA}}, \quad (28)$$

$$\text{s.t.} \quad -\frac{\pi}{2} \leq \omega \leq \frac{\pi}{2}, \quad (29)$$

$$-\frac{\pi}{2} \leq \gamma \leq \frac{\pi}{2}, \quad (30)$$

$$1.5 \leq \eta_c \leq 1.7, \quad (31)$$

where the constraints (29) and (30) denote the bounds of the roll angle and yaw angle, respectively, of the mirror array-based OSTAR-RIS elements. Constraint (31) denotes the bound of the LC-based OSTAR-RIS elements. (P0) requires the joint optimization of all three optimization variables. Besides, it is highly non-convex. Subsequently, it cannot be solved using traditional optimization methods. To get the global optimal solution of (P0), we resort to the sine-cosine algorithm (SCA) [42], which is a population-based meta-heuristic algorithm. The merits of the SCA methods are as follows, (i) ability to avoid being trapped in a local maxima (i.e., a sub-optimal solution), (ii) fast convergence, (iii) ease of implementation, and (iv) fewer parameters.

B. Proposed Solution Methodology

The SCA, a method based on iterative population search, was developed by Mirjalili [42] and has recently found applications in wireless communications [2], [16], [30], [43], [44], remote sensing [45], and electrical power system design [46], [47] due to its ability to obtain the global optimal solution for complex optimization problems. According to this method, G search agents are randomly deployed within the boundary of the search space of the optimization problem. The position of each agent represents a candidate solution to the optimization problem and gets updated via mathematical models based on the sine and cosine functions. Thus, the agents explore the search space in parallel to find the promising regions by using the sine function and then exploit those regions to obtain the overall best solution via the cosine function. At iteration t , the solution of agent g is denoted as $s_g^t = [\omega, \gamma, \eta_c]$ and its fitness can be determined via the objective function (28). The fitness of the agents is evaluated using the objection function and the current best solution among them at iteration t (i.e., fittest agent), called destination point, is denoted as \mathcal{D}^t . It is called a destination point since the other agents would try to get to that position in the next iteration. At the $t+1$ -th iteration, the solution of the v -th variable of each agent is updated as follows [42]

$$s_{g,v}^{t+1} = \begin{cases} s_{g,v}^t + r_1 \times \cos(r_2) \times |r_3 \mathcal{D}^t - s_{g,v}^t|, & \text{if } r_4 \geq 0.5 \\ s_{g,v}^t + r_1 \times \sin(r_2) \times |r_3 \mathcal{D}^t - s_{g,v}^t|, & \text{if } r_4 < 0.5 \end{cases} \quad (32)$$

where r_1, r_2, r_3 and r_4 are the main parameters that influence the search procedure of the SCA and $|\cdot|$ denotes the absolute value. Specifically

$$r_1 = \tilde{a} - t(\tilde{a}/T), \quad (33)$$

with \tilde{a} being a constant and T being the maximum number of iterations, can adaptively guide the movement direction

Algorithm 1: Proposed solution for optimization problem (P0).

Input: $G, T, \tilde{a}, V, V_{TH}, V_E, V_0, \rho_{RIS}, \eta_e, \eta_a, \eta_o$;
Output: The optimal yaw and roll angles and the refractive index γ^*, ω^* , and η_c^* , respectively;

- 1 Initialize $t = 0$ and $s_{g,v}^t, \forall g$;
- 2 Compute the fitness of each agent via (18) or (27);
- 3 Set \mathcal{D}^t as the solution of the fittest agent;
- 4 Update $t = t + 1$;
- 5 **while** *No convergence* **do**
- 6 Obtain r_1, r_2, r_3, r_4 ;
- 7 **for** $g = 1 : G$ **do**
- 8 **for** $v = 1 : 3$ **do**
- 9 Update $s_{g,v}^t, \forall g$ by solving (32);
- 10 **end**
- 11 **end**
- 12 Check agents for constraint(s) violation;
- 13 Update the fitness of each agent using (18) or (27);
- 14 Update \mathcal{D}^t ;
- 15 Update $t = t + 1$;
- 16 **end**

of the search agents (i.e., the location to be searched in the next iteration). The global exploitation and local exploration abilities of the SCA are emphasized when $r_1 > 1$ and $r_1 \leq 1$, respectively. As evident from (33), the value of r_1 is larger during the early stage of the algorithm (since t is small), which enables excellent global exploitation. As t gets larger, the value of r_1 decreases, which allows the algorithm to thoroughly search (i.e., local exploration) around the current best solution for the global optimal solution. The parameter r_2 controls the movement distance towards or outwards the destination point and its value is selected randomly from the interval $(0, 2\pi)$. The parameter r_3 determines the extent to which the destination point affects the distance between the current solution and the destination point and its value is randomly chosen according to a uniform distribution in the interval $(0, 2)$. Lastly, the parameter r_4 which takes on a random value in the interval $(0, 1)$ switches with equal probability between the sine and cosine functions. The components $r_1 \times \sin(r_2)$ and $r_1 \times \cos(r_2)$ jointly enhance the exploration (when these two values are greater than 1 or less than -1) and exploitation (when these two values fall within the range of -1 to 1) during the search process. In summary, the parameters r_1, r_2, r_3 , and r_4 are used to iteratively guide the movement of the agents in the search space to achieve a good balance between exploration (covering a wide range of solutions) and exploitation (focusing on promising solutions). For each iterate, the fitness of all agents is determined and the fittest serves as the new destination point. This repeats until a predefined termination criterion is met. Algorithm 1 summarizes the proposed SCA-based algorithm.

C. Computational Complexity Analysis

The time complexity of Algorithm 1 mainly depends on (i) the generation of the initial set of solutions for all agents, (ii) the evaluation of the fitness of the solution of all agents, (iii) the selection of the destination point, (iv) updating the agents' solutions, and (v) the total number of iterations. The corresponding time complexities of the tasks mentioned in (i), (ii), (iii), and (iv) are $\mathcal{O}(GV)$, $\mathcal{O}(G)$, $\mathcal{O}(G)$, and $\mathcal{O}(GVT)$, respectively, where V denotes the total number of decision

variables. As a result, the worst-case computational complexity of Algorithm 1 is $\mathcal{O}(GVT)$.

V. SUM ENERGY EFFICIENCY OPTIMIZATION

The SEE metric has gained widespread use as a performance metric in VLC systems [16], [48], [49]. It can be defined as the ‘‘ratio between the sum rate of the VLC system and the total power the system consumes’’, and is typically measured in Bits per Joule. The sum rate of the proposed system, for the power-domain NOMA and the RSMA schemes, are detailed in (18) and (27), respectively. The total consumed power of the proposed system encompasses various components: Firstly, the consumed power at the VLC AP can be expressed as [16]

$$\mathcal{P}_{\text{VLC-AP}} = \mathcal{P}_{\text{T-Circuit}} + \mathcal{P}_{\text{Driver}} + \mathcal{P}_{\text{PA}} + \mathcal{P}_{\text{Filter}} + \mathcal{P}_{\text{DAC}} + \mathcal{P}_{\text{S}}, \quad (34)$$

where $\mathcal{P}_{\text{T-Circuit}}$ denotes the power of the transmitter external circuit, $\mathcal{P}_{\text{Driver}}$ denotes the power of the LED driver, \mathcal{P}_{PA} denotes the power of the power amplifier, $\mathcal{P}_{\text{Filter}}$ denotes the power of the filter, \mathcal{P}_{DAC} denotes the power of the digital-to-analog converter (DAC), and \mathcal{P}_{S} denotes the power of the signal. Secondly, the power consumed at the OSTAR-RIS can be expressed as

$$\mathcal{P}_{\text{OSTAR-RIS}} = \mathcal{P}_m \times \mathcal{K} + \mathcal{P}_{\text{LC}} \times \mathcal{N}, \quad (35)$$

where \mathcal{P}_m denotes the power of each mirror array-based reflector element, and \mathcal{P}_{LC} denotes the power of each LC-based refractor element. Lastly, the power consumption at the receiver can be expressed as [16]

$$\mathcal{P}_{\text{R}} = \mathcal{P}_{\text{R-Circuit}} + \mathcal{P}_{\text{Filter}} + \mathcal{P}_{\text{TIA}} + \mathcal{P}_{\text{ADC}}, \quad (36)$$

where $\mathcal{P}_{\text{R-Circuit}}$ denotes the power of the receiver external circuit, \mathcal{P}_{TIA} denotes the power of the trans-impedance amplifier (TIA), and \mathcal{P}_{ADC} denotes the power of the analog-to-digital converter (ADC). Overall, the total consumed power of the proposed system can be given as

$$\mathcal{P}_{\text{Total}} = \mathcal{P}_{\text{T}} + \mathcal{P}_{\text{OSTAR-RIS}} + \mathcal{P}_{\text{R}}. \quad (37)$$

Consequently, the SEE of the proposed system, for the power-domain NOMA and the RSMA schemes, can be formulated, respectively, as

$$\begin{aligned} \text{SEE}^{\text{NOMA}} &= \frac{P_{\text{sum}}^{\text{NOMA}}}{\mathcal{P}_{\text{Total}}}, \\ \text{SEE}^{\text{RSMA}} &= \frac{P_{\text{sum}}^{\text{RSMA}}}{\mathcal{P}_{\text{Total}}}. \end{aligned} \quad (38)$$

To maximize the SEE metric, the objective function of (P0) is replaced by (38). Then, the resultant optimization problem is solved using similar procedures to the ones outlined in Section IV-B.

VI. SIMULATION RESULTS

This section presents extensive numerical simulations to assess the performance of the proposed OSTAR-RIS-aided VLC system under both the power-domain NOMA and the RSMA schemes. Table II summarizes the default parameters used during the simulations. Beyond this list, the polar angle, α , and the azimuth angle, β , are characterized using the

Table II
SIMULATION PARAMETERS

Parameter	Value	Parameter	Value
$\Phi_{1/2}$	70°	A_{PD}	1.0 cm^2
$T(\xi)$	1.0	d	2.5 m
f	1.5	ξ_{FoV}	85°
ρ_{RIS}	0.95	ρ_{wall}	0.8
η_e	1.7	η_a	1.0
V_{TH}	1.34 V	η_o	1.5
D	0.75 mm	V_0	1.0 V
r_{eff}	12 pm/V	λ	{510, 670} nm
q	3.0	B	200 MHz
N_o	$10^{-21} \text{ A}^2/\text{Hz}$	R_{PD}	0.53 A/W
V	3	G	5
T	4000	\bar{a}	2.0
U	4	$\{\mu^{\text{NOMA}}, \mu^{\text{RSMA}}\}$	{0.6, 0.6}
P_{tot}	10 dBm	p	{1, 1.5, ..., 4} Watt
P_{ADC}	95 mWatt	P_{DAC}	175 mWatt
P_{Driver}	2758 mWatt	P_{Filter}	2.5 mWatt
P_m	100 mWatt	P_{TIA}	2500 mWatt
$P_{\text{R-Circuit}}$	1.9 mWatt	$P_{\text{T-Circuit}}$	3250 mWatt
P_{LC}	320 mWatt	P_{PA}	280 mWatt

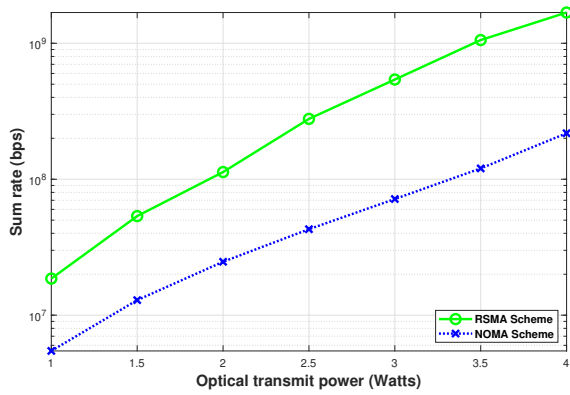


Fig. 2. Sum rate versus AP optical transmit power. At $\lambda = 510$ nm.

uniform distribution within the range of $[-\pi, \pi]$ and the Laplace distribution within the range of $[0, \frac{\pi}{2}]$, respectively. The system depicts users as cylindrical objects with a height of 1.65 meters and a diameter of 0.3 meters, with a receiver that is located 0.36 meters away from their body at a height of 0.85 meters. Both Rooms 1 and 2 have a dimension of $5.0 \times 5.0 \times 3.0$ meters with an AP fixed at the center of Room 1. The OSTAR-RIS comprises 5 rows and 10 columns with 25 LC-based elements and 25 mirror array-based elements, unless otherwise specified. Each element is a square that spans over $0.1 \text{ m} \times 0.1 \text{ m}$. In this section, we set ι in (1) to zero, as we focus on the NLoS scenario. The parameters utilized in this section are extracted from [2], [13], [16], [30], [34], [39], [49].

Fig. 2 compares the sum rate performance of the proposed OSTAR-RIS-assisted multi-user indoor VLC system for the RSMA scheme and the power-domain NOMA scheme for different AP optical transmit powers. It can be observed that the sum-rate performance of RSMA-aided system is superior to the corresponding NOMA-aided system with an enhancement in the sum rate that is up to 456%. This illustrates that adopting the RSMA scheme is more spectrally efficient for the proposed OSTAR-RIS-assisted VLC system (i.e., achieves higher data performance with the same resources) than the power-domain NOMA scheme.

Fig. 3 compares the sum rate performance of the proposed OSTAR-RIS-assisted multi-user indoor VLC system for the

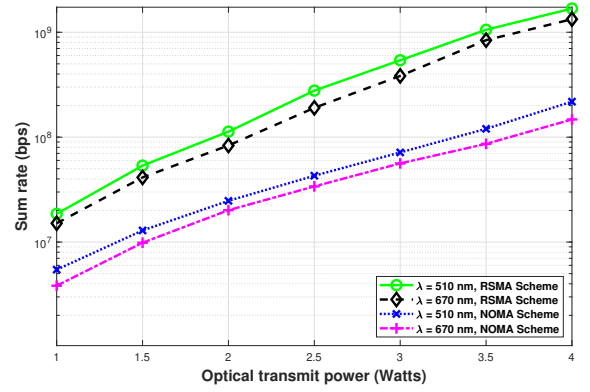


Fig. 3. Sum rate versus wavelength of the transmitted light signal. At $p = 3$ Watts.

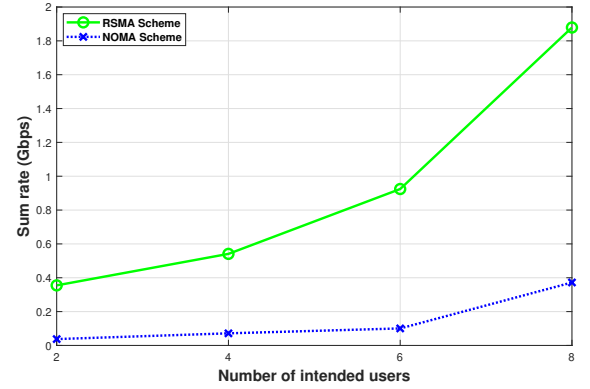


Fig. 4. Sum rate versus number of intended users. At $\lambda = 510$ nm, and $p = 3$ Watts.

RSMA scheme and the power-domain NOMA scheme for different wavelength of the transmitted light signal. This figure is generated because altering the wavelengths affects the sum-rate performance of the LC-based OSTAR-RIS elements [16], [30] (i.e., based on (13), as the wavelength increases, the amplification gain coefficient, Γ , decreases and subsequently, the sum rate performance deteriorates). This figure shows a sum-rate deterioration up to 31% and 29% in RSMA-aided system and power-domain NOMA-aided system, respectively, when the wavelength of the transmitted light signal is changed from 510 nm to 670 nm.

Fig. 4 shows the sum rate performance of the proposed OSTAR-RIS-assisted multi-user indoor VLC system for the RSMA scheme and the power-domain NOMA scheme versus the number of users in the system. Clearly, the sum rate performance of the RSMA-aided system outperforms the NOMA-aided system. This is because the multiuser gain is higher in the RSMA scheme than in the power-domain NOMA scheme.

In Fig. 5, the sum rate performance of the proposed OSTAR-RIS-assisted multi-user indoor VLC system for the RSMA scheme under three power allocation strategies is illustrated. Specifically, (i) equal power allocation strategy (adopted strategy) (i.e., distributing the power of the private streams equally), (ii) the NOMA-alike power allocation strategy (i.e., distributing the power of the private streams using the same strategy utilized in the power-domain NOMA scheme based

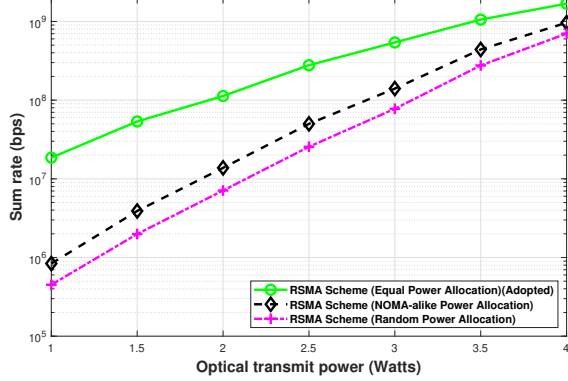


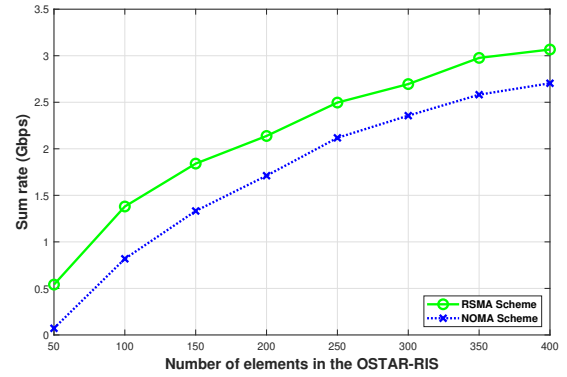
Fig. 5. Sum rate versus AP optical transmit power for different power allocation strategies for the RSMA scheme. At $\lambda = 510$ nm and $p = 3$ Watts.

on (16)) and (ii) the random power allocation (i.e., distributing the power of the private streams based on uniform random distribution). From this figure, it is evident that the RSMA scheme achieves the best sum rate performance using (i). This is because the power allocation strategy in (ii) is designed for the NOMA scheme and the power allocation strategy in (iii) might not utilize the whole portion of power dedicated to the private streams.

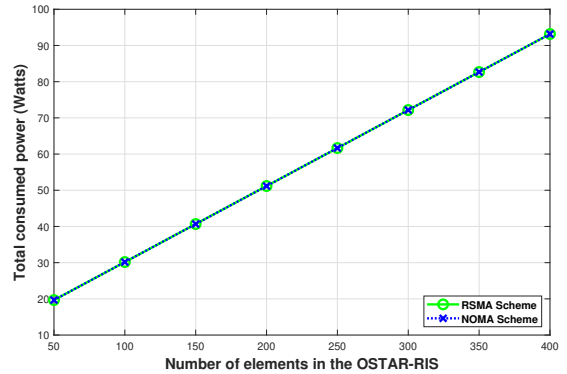
Fig. 6 demonstrates the sum rate, total consumed-power, and sum energy efficiency performance of the proposed OSTAR-RIS-assisted multi-user indoor VLC system for the RSMA scheme and the power-domain NOMA scheme versus the number of elements in the OSTAR-RIS. Fig. 6a reveals that as the number of elements in the OSTAR-RIS increases the sum rate performance of both the RSMA and the power-domain NOMA schemes increases. It is worth mentioning that the percentage of this increase here is slower than the one in, for example, Fig. 2. This can be justified by the fact that introducing additional elements to a sizable OSTAR-RIS results in minimal improvement. Fig. 6b shows that the total consumed-power is identical for both the RSMA scheme and the power-domain NOMA scheme as the parameters related to both mentioned schemes are not factors in (37). By examining Fig. 6c, it is apparent that the enhancement in the SEE initially increases with the growing number of elements in the OSTAR-RIS, but eventually declines. This pattern can be explained as follows: the system's sum rate (as shown in Fig. 6a) logarithmically increases and the total consumed power of the proposed system (as depicted in Fig. 6b) linearly increases while increasing the number of OSTAR-RIS elements.

VII. CONCLUSION

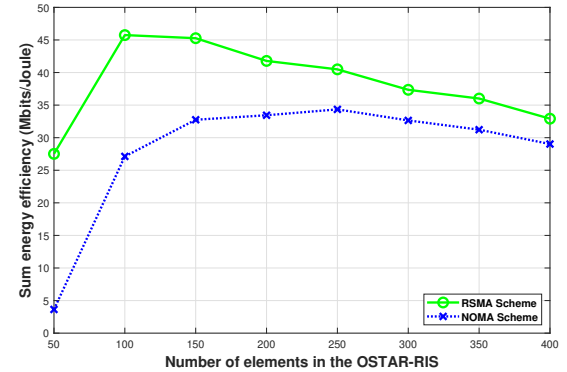
This paper proposes and investigates a novel multi-user indoor VLC system that is assisted by OSTAR-RIS. The proposed system combats challenging LoS blockage scenarios resulting from (i) other users (i.e., blockers), (ii) walls within the indoor environment, and (iii) the orientation of the recipient's device. For the proposed system, both the sum rate and the SEE optimization problems, for both the power-domain NOMA and the RSMA schemes, are formulated, solved, and evaluated. These optimization problems jointly design the roll and yaw angles of the mirror array-based



(a) Sum rate.



(b) Total consumed power.



(c) Sum energy efficiency.

Fig. 6. Proposed OSTAR-RIS-assisted multi-user indoor VLC system's performance versus number of OSTAR-RIS elements. At $\lambda = 510$ nm and $p = 3$ Watts.

OSTAR-RIS elements as well as the refractive index of the LC-based OSTAR-RIS elements. The sine-cosine meta-heuristic algorithm is utilized to get the global optimal solution for both formulated multi-variate non-convex optimization problems. Detailed simulation results are provided to illustrate the superiority of the RSMA scheme over the power-domain NOMA scheme for the proposed system in terms of both the sum rate and the SEE metrics while considering different network parameters such as the AP optical transmit power, the wavelength of the transmitted light, the number of elements in the OSTAR-RIS, and the number of served users. In addition, the effect of adopting different power allocation strategies on the sum rate performance of the RSMA scheme is illustrated.

REFERENCES

- [1] S. Al-Ahmadi, O. Maraqa, M. Uysal, and S. M. Sait, "Multi-user visible light communications: State-of-the-art and future directions," *IEEE Access*, vol. 6, pp. 70 555–70 571, 2018.
- [2] S. Aboagye, T. M. N. Ngatched, O. A. Dobre, and A. R. Ndjiongue, "Intelligent reflecting surface-aided indoor visible light communication systems," *IEEE Commun. Lett.*, vol. 25, no. 12, pp. 3913–3917, Dec. 2021.
- [3] S. Sun, F. Yang, and J. Song, "Sum rate maximization for intelligent reflecting surface-aided visible light communications," *IEEE Commun. Lett.*, vol. 25, no. 11, pp. 3619–3623, Nov. 2021.
- [4] L. Qian, X. Chi, L. Zhao, and A. Chaaban, "Secure visible light communications via intelligent reflecting surfaces," in *IEEE Int. Conf. Commun. (ICC 2021)*, Jun. 2021, pp. 1–6.
- [5] H. Abumarshoud, C. Chen, I. Tavakkolnia, H. Haas, and M. A. Imran, "Intelligent reflecting surfaces for enhanced physical layer security in NOMA VLC systems," in *IEEE Int. Conf. Commun. (ICC 2023)*, May 2023, pp. 3284–3289.
- [6] S. Sun, F. Yang, J. Song, and Z. Han, "Joint resource management for intelligent reflecting surface-aided visible light communications," *IEEE Trans. Wirel. Commun.*, vol. 21, no. 8, pp. 6508–6522, Aug. 2022.
- [7] S. Sun, F. Yang, J. Song, and R. Zhang, "Intelligent reflecting surface for MIMO VLC: Joint design of surface configuration and transceiver signal processing," *IEEE Trans. Wirel. Commun.*, vol. 22, no. 9, pp. 5785–5799, Sep. 2023.
- [8] Q. Wu, J. Zhang, Y. Zhang, G. Xin, and J. Guo, "Configuring reconfigurable intelligent surface for parallel MIMO visible light communications with asymptotic capacity maximization," *Appl. Sci.*, vol. 13, no. 1, p. 563, Dec. 2022.
- [9] X.-D. Shi, L.-H. Hong, P.-F. Yu, J.-W. Shi, N. Liu, and J.-Y. Wang, "Performance analysis and parameter optimization for intelligent reflecting mirror array-aided visible light communications," *J. Opt. Soc. Am. A*, vol. 39, no. 10, pp. 1839–1848, Oct. 2022.
- [10] T. Yang, P. Wang, G. Li, H. Wang, S. Li, H. Shi, H. He, F. Shi, and S. Chi, "Average signal-to-noise ratio maximization for an intelligent reflecting surface and angle diversity receiver jointly assisted indoor visible light communication system," *Appl. Opt.*, vol. 61, no. 35, pp. 10 390–10 399, Dec. 2022.
- [11] D. A. Saifaldeen, B. S. Ciftler, M. M. Abdallah, and K. A. Qaraqe, "DRL-based IRS-assisted secure visible light communications," *IEEE Photonics J.*, vol. 14, no. 6, pp. 1–9, Dec. 2022.
- [12] S. Sun, F. Yang, J. Song, and Z. Han, "Optimization on multiuser physical layer security of intelligent reflecting surface-aided VLC," *IEEE Wireless Commun. Lett.*, vol. 11, no. 7, pp. 1344–1348, Jul. 2022.
- [13] L. Zhan, H. Zhao, W. Zhang, and J. Lin, "An optimal scheme for the number of mirrors in vehicular visible light communication via mirror array-based intelligent reflecting surfaces," in *Photonics*, vol. 9, no. 3, MDPI, Feb. 2022, p. 129.
- [14] Q. Wu, J. Zhang, and J. Guo, "Capacity maximization for reconfigurable intelligent surface-aided MISO visible light communications," in *Photonics*, vol. 9, no. 7, MDPI, Jul. 2022, p. 487.
- [15] Q. Wu, J. Zhang, and J.-N. Guo, "Position design for reconfigurable intelligent-surface-aided indoor visible light communication systems," *Electronics*, vol. 11, no. 19, p. 3076, Sep. 2022.
- [16] O. Maraqa and T. M. N. Ngatched, "Optimized design of joint mirror array and liquid crystal-based RIS-aided VLC systems," *IEEE Photon. J.*, vol. 15, no. 4, pp. 1–11, Jul. 2023.
- [17] S. Sun, W. Mei, F. Yang, N. An, J. Song, and R. Zhang, "Optical intelligent reflecting surface assisted MIMO VLC: Channel modeling and capacity characterization," *IEEE Trans. Wirel. Commun.*, pp. 1–1, Jul. 2023.
- [18] B. Cao, M. Chen, Z. Yang, M. Zhang, J. Zhao, and M. Chen, "Reflecting the light: Energy efficient visible light communication with reconfigurable intelligent surface," in *IEEE Veh. Technol. Conf. (VTC2020-Fall)*, Nov. 2020, pp. 1–5.
- [19] C. Liu, L. Yu, X. Yu, J. Qian, Y. Wang, and Z. Wang, "Capacity analysis of RIS-assisted visible light communication systems with hybrid NOMA," in *IEEE Glob. Commun. (2022GC Wkshps)*, Dec. 2022, pp. 118–123.
- [20] H. Abumarshoud, B. Selim, M. Tatipamula, and H. Haas, "Intelligent reflecting surfaces for enhanced NOMA-based visible light communications," in *IEEE Int. Conf. Commun. (ICC 2022)*, May 2022, pp. 571–576.
- [21] Z. Liu, F. Yang, S. Sun, J. Song, and Z. Han, "Sum rate maximization for NOMA-based VLC with optical intelligent reflecting surface," *IEEE Wireless Commun. Lett.*, vol. 12, no. 5, pp. 848–852, May 2023.
- [22] A. Mukherjee, V. Kumar, D. W. K. Ng, and L.-N. Tran, "On the energy-efficiency maximization for IRS-assisted MIMOME wiretap channels," in *IEEE Veh. Technol. Conf. (VTC2022-Fall)*, Sep. 2022, pp. 1–6.
- [23] A. Salehiyan and M. J. Emadi, "Performance analysis of uplink optical wireless communications in the presence of a simultaneously transmitting and reflecting reconfigurable intelligent surface," *IET Optoelectron.*, May 2023.
- [24] A. M. Abdelhady, A. K. S. Salem, O. Amin, B. Shihada, and M.-S. Alouini, "Visible light communications via intelligent reflecting surfaces: Metasurfaces vs mirror arrays," *IEEE Open J. Commun. Soc.*, vol. 2, pp. 1–20, 2021.
- [25] A. R. Ndjiongue, T. M. N. Ngatched, O. A. Dobre, H. Haas, and H. Shin, "Double-sided beamforming in VLC systems using omni-digital reconfigurable intelligent surfaces," *IEEE Commun. Mag.*, pp. 1–7, early access, 2023.
- [26] Y. Mao, O. Dizdar, B. Clerckx, R. Schober, P. Popovski, and H. V. Poor, "Rate-splitting multiple access: Fundamentals, survey, and future research trends," *IEEE Commun. Surv. Tutor.*, vol. 24, no. 4, pp. 2073–2126, Fourthquarter 2022.
- [27] B. Clerckx, Y. Mao, E. A. Jorswieck, J. Yuan, D. J. Love, E. Erkip, and D. Niyato, "A primer on rate-splitting multiple access: Tutorial, myths, and frequently asked questions," *IEEE J. Sel. Areas Commun.*, vol. 41, no. 5, pp. 1265–1308, May 2023.
- [28] T. Komine and M. Nakagawa, "Fundamental analysis for visible-light communication system using LED lights," *IEEE Trans. Consum. Electron.*, vol. 50, no. 1, pp. 100–107, Feb. 2004.
- [29] M. D. Soltani, A. A. Purwita, Z. Zeng, H. Haas, and M. Safari, "Modeling the random orientation of mobile devices: Measurement, analysis and LiFi use case," *IEEE Trans. Commun.*, vol. 67, no. 3, pp. 2157–2172, Mar. 2019.
- [30] S. Aboagye, A. R. Ndjiongue, T. M. N. Ngatched, and O. A. Dobre, "Design and optimization of liquid crystal RIS-based visible light communication receivers," *IEEE Photonics J.*, vol. 14, no. 6, pp. 1–7, 2022.
- [31] B. E. Saleh and M. C. Teich, *Fundamentals of Photonics*. New York, USA: John Wiley & Sons, Feb. 2019.
- [32] W. Demtröder, *Laser Spectroscopy 1: Basic Principles*. Berlin/Heidelberg, Germany: Springer, 2014.
- [33] V. Marinova, S. Huei Lin, R. Chung Liu, and K. Y. Hsu, "Photorefractive Effect: Principles, Materials, and Near-Infrared Holography," *Wiley Encyclopedia of Electrical and Electronics Engineering*, pp. 1–20, 1999.
- [34] O. Maraqa, U. F. Siddiqi, S. Al-Ahmadi, and S. M. Sait, "On the achievable max-min user rates in multi-carrier centralized NOMA-VLC networks," *Sensors*, vol. 21, no. 11, p. 3705, May 2021.
- [35] O. Maraqa, A. S. Rajasekaran, S. Al-Ahmadi, H. Yanikomeroğlu, and S. M. Sait, "A survey of rate-optimal power domain NOMA with enabling technologies of future wireless networks," *IEEE Commun. Surv. Tutor.*, vol. 22, no. 4, pp. 2192–2235, Fourthquarter 2020.
- [36] X. Zhang, Q. Gao, C. Gong, and Z. Xu, "User grouping and power allocation for NOMA visible light communication multi-cell networks," *IEEE Commun. Lett.*, vol. 21, no. 4, pp. 777–780, Apr. 2017.
- [37] T. Shen, V. Yachongka, Y. Hama, and H. Ochiai, "Secrecy design of indoor visible light communication network under downlink NOMA transmission," *arXiv preprint arXiv:2304.08458*, Apr. 2023.
- [38] Z. Yang, M. Chen, W. Saad, and M. Shikh-Bahaei, "Optimization of rate allocation and power control for rate splitting multiple access (RSMA)," *IEEE Trans. Commun.*, vol. 69, no. 9, pp. 5988–6002, Sep. 2021.
- [39] M. A. Saeidi and H. Tabassum, "Resource allocation and performance analysis of hybrid RSMA-NOMA in the downlink," *arXiv preprint arXiv:2306.08781*, Jun. 2023.
- [40] Y. Mao, B. Clerckx, J. Zhang, V. O. K. Li, and M. A. Arafah, "Max-min fairness of k -user cooperative rate-splitting in MISO broadcast channel with user relaying," *IEEE Trans. Wirel. Commun.*, vol. 19, no. 10, pp. 6362–6376, Oct. 2020.
- [41] K. D. Alazwary, A. Adnan Qidan, T. E. H. El-Gorashi, and J. M. H. Elmighani, "Rate splitting for 6G optical wireless networks," in *2023 23rd Int. Conf. on Trans. Opt. Net. (ICTON)*, Aug. 2023, pp. 1–5.
- [42] S. Mirjalili, "SCA: A sine cosine algorithm for solving optimization problems," *Knowl. Based Syst.*, vol. 96, pp. 120–133, Mar. 2016.
- [43] J. Chen, X. Li, J. Xu, and Y. Wang, "Deployment for NOMA-UAV base stations based on hybrid sparrow search algorithm," *IEEE Trans. Aerosp. Electron. Syst.*, vol. 59, no. 5, pp. 6138–6149, Oct. 2023.
- [44] Y. Wang, X. Han, and S. Jin, "Performance analysis of a VM-PM repair strategy in MEC-enabled wireless systems with bursty traffic," *IEEE Trans. Veh. Technol.*, pp. 1–16, Early Access 2023.

- [45] Y. Wan, A. Ma, L. Zhang, and Y. Zhong, "Multiobjective sine cosine algorithm for remote sensing image spatial-spectral clustering," *IEEE Trans. Cybern.*, vol. 52, no. 10, pp. 11 172–11 186, Oct. 2022.
- [46] M. S. Saddique, S. Habib, S. S. Haroon, A. R. Bhatti, S. Amin, and E. M. Ahmed, "Optimal solution of reactive power dispatch in transmission system to minimize power losses using sine-cosine algorithm," *IEEE Access*, vol. 10, pp. 20 223–20 239, 2022.
- [47] S. Padmanaban, N. Priyadarshi, J. B. Holm-Nielsen, M. Sagar Bhaskar, F. Azam, A. K. Sharma, and E. Hossain, "A novel modified sine-cosine optimized MPPT algorithm for grid integrated PV system under real operating conditions," *IEEE Access*, vol. 7, pp. 10 467–10 477, 2019.
- [48] S. Aboagye, T. M. N. Ngatched, O. A. Dobre, and A. G. Armada, "Energy efficient subchannel and power allocation in cooperative VLC systems," *IEEE Commun. Lett.*, vol. 25, no. 6, pp. 1935–1939, Jun. 2021.
- [49] S. Ma, T. Zhang, S. Lu, H. Li, Z. Wu, and S. Li, "Energy efficiency of SISO and MISO in visible light communication systems," *J. Light. Technol.*, vol. 36, no. 12, pp. 2499–2509, Jun. 2018.



Telex M. N. Ngatched (Senior Member, IEEE) received the B.Sc. degree and the M.Sc. degree in electronics from the University of Yaoundé, Cameroon, in 1992 and 1993, respectively, the MscEng (Cum Laude) in electronic engineering from the University of Natal, Durban, South Africa, in 2002, and the Ph.D. in electronic engineering from the University of KwaZulu-Natal, Durban, South Africa, in 2006. From July 2006 to December 2007, he was with the University of KwaZulu-Natal as a Postdoctoral Fellow, from 2008 to 2012 with the Department of Electrical and Computer Engineering, University of Manitoba, Canada, as a Research Associate, and from 2012 to 2022 with Memorial University. He joined McMaster University in January 2023, where he is currently an Associate Professor. His research interests include 5G and 6G enabling technologies, optical wireless communications, hybrid optical wireless and radio frequency communications, artificial intelligence and machine learning for communications, and underwater communications.

Dr. Ngatched serves as an Area Editor for the IEEE Open Journal of the Communications Society, an Associate Technical Editor for the IEEE Communications Magazine, and an Editor of the IEEE Communications Society On-Line Content. He was the publication chair of the IEEE CWIT 2015, the Managing Editor of the IEEE Communications Letters and IEEE Communications Magazine, an Associate Editor of the IEEE Open Journal of the Communications Society and IEEE Communications Letters, the co-chair of the Spectrum Management, Radio Access technology, Services and Security track of VTC2021-Spring and VTC2022-Spring, and Technical Program Committee (TPC) member and session chair for many prominent IEEE conferences including GLOBECOM, ICC, WCNC, VTC, and PIMRC. He was a recipient of the Best Paper Award at the IEEE Wireless Communications and Networking Conference (WCNC) in 2019. He is a Professional Engineer (P. Eng.) registered with the Professional Engineers Ontario, Toronto, ON, Canada.



Omar Maraqa has received his B.S. degree in Electrical Engineering from Palestine Polytechnic University, Palestine, in 2011, his M.S. degree in Computer Engineering from King Fahd University of Petroleum & Minerals (KFUPM), Dhahran, Saudi Arabia, in 2016, and his Ph.D. degree in Electrical Engineering at KFUPM, Dhahran, Saudi Arabia, in 2022. He is currently a Postdoctoral Research Fellow with the Department of Electrical and Computer Engineering, at McMaster University, Canada. His research interests include performance analysis and

optimization of wireless communications systems.



Sylvester Aboagye (Member, IEEE) received the B.Sc. degree (Hons.) in telecommunication engineering from the Kwame Nkrumah University of Science and Technology, Kumasi, Ghana, in 2015, and the M.Eng. and Ph.D. degrees in electrical engineering from Memorial University, St. John's, NL, Canada, in 2018 and 2022, respectively. He is currently a Postdoctoral Research Fellow with the Department of Electrical Engineering and Computer Science at York University, Canada. His current research interests include the design and optimization

of multiband wireless communication systems, terrestrial and non-terrestrial integrated sensing and communication networks, and 6G and beyond enabling technologies.